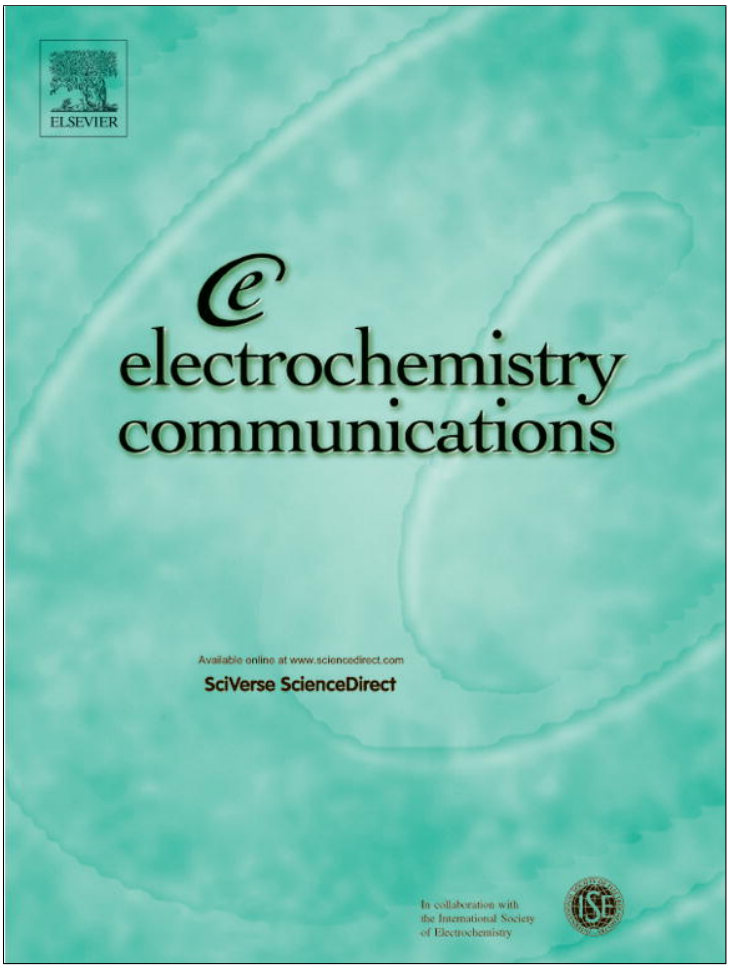

Electrochemistry Communications 34 (2013) 231–234

Contents lists available at SciVerse ScienceDirect

Electrochemistry Communications

journal homepage: www.elsevier.com/locate/elecom

Short communication

Intermediate temperature micro-tubular SOFCs with enhanced performance and thermal stability

Chenghao Yang [a,*], Chao Jin [b], Meilin Liu [a,c], Fanglin Chen [d,*]

[a] New Energy Research Institute, College of Environment and Energy, South China University of Technology, Guangzhou 510006, PR China
[b] School of Energy, Soochow University, Suzhou, Jiangsu 215006, PR China
[c] School of Materials Science & Engineering, Georgia Institute of Technology, Atlanta, GA 30332-0245, USA
[d] Department of Mechanical Engineering, University of South Carolina, Columbia, SC 29208, USA

ARTICLE INFO

Article history:
Received 28 April 2013
Received in revised form 18 June 2013
Accepted 18 June 2013
Available online 26 June 2013

Keywords:
Micro-tubular solid oxide fuel cell
Phase-inversion
Co-sintering
Impregnation

ABSTRACT

Anode supported intermediate temperature micro-tubular solid oxide fuel cells (MT-SOFCs) with the cell configuration of Ni-Sc_2O_3 stabilized ZrO_2 (ScSZ)/ScSZ/$(La_{0.75}Sr_{0.25})_{0.95}MnO_3$ (LSM)-$Sm_{0.2}Ce_{0.8}O_{1.9}$ (SDC)-ScSZ have been fabricated by a combination of phase-inversion, dip-coating, co-sintering and impregnation method. Cross-sectional SEM images of the fabricated MT-SOFC reveal that the dense ScSZ electrolyte and porous ScSZ backbone in the anode and cathode formed together, and the stability test demonstrates that the fabricated MT-SOFCs have robust resistance to thermal cycling. Maximum power densities of 0.29, 0.40 and 0.52 W cm^{-2} have been achieved at 550, 600 and 650 °C, respectively. The results indicate that the fabricated MT-SOFC has potential applications for portable power needs.

1. Introduction

Solid oxide fuel cells (SOFCs) are promising energy conversion devices that can convert the chemical energy in the fuel directly to electricity with high energy conversion efficiency and fuel flexibility [1,2]. Currently, the most widely used configurations for SOFCs are planar and tubular, both of them employing a structure in which a dense solid electrolyte is sandwiched between two porous electrodes. However, due to the brittleness and thermal expansion coefficient (TEC) mismatch among the cell components, fast degradation caused by rapid heating from room temperature to high operating temperature (800–900 °C) is a significant challenge [3,4], and a slow heating up and/or cooling down are therefore required. Moreover, the high operating temperature significantly limits the choice of the cell materials, which must possess sufficient chemical and thermal stability under the operating conditions [5–7]. In order to develop SOFCs for a broad spectrum of power generation applications such as auxiliary power units for transportations and portable power devices for consumer electronics, it is desirable to reduce the operating temperature and improve the thermal cycling robustness of the SOFCs [8]. Recently, intermediate temperature micro-tubular SOFC (MT-SOFC) has attracted considerable interests due to its high resistance to thermal stress caused by quick startup and/or shut down operations, and characteristic high volumetric power density compared with the conventional tubular or planar SOFCs [9,10].

In general, anode support for MT-SOFCs has been fabricated by extrusion [11], isostatic pressing [12] and casting method [13]. Recently, phase-inversion method, a relatively simple process involving no expensive equipment has been utilized to fabricate ceramic hollow fiber membranes for applications in MT-SOFCs [10,14]. Although significant progress has been made on MT-SOFCs, there have been very few reports in optimizing electrochemical performance and mechanical durability simultaneously. In this work, we have made further improvements to fabricate MT-SOFCs, lowering their operating temperature down to 550–650 °C and enhancing their thermal stability. Phase-inversion, dip coating and co-sintering have been applied to fabricate Ni-scandia stabilized zirconia (ScSZ)(porous)/ScSZ(dense)/ScSZ(porous) tri-layer ceramic structure. The co-sintering process results in dense ScSZ electrolyte and porous ScSZ backbone in the anode and cathode together, establishing a bridge between the electrodes and the electrolyte, which will not only provide an optimum interface for oxygen ion conduction, but also greatly improve the cell resistance to thermal cycling. Nano-sized $(La_{0.75}Sr_{0.25})_{0.95}MnO_3$ (LSM) and $Sm_{0.2}Ce_{0.8}O_{1.9}$ (SDC) catalysts have subsequently been loaded into the porous ScSZ matrix through an impregnation method, to enlarge the length of catalyst/ScSZ/gas and SDC/catalyst/gas three phase boundary (TPB) in the cathode for cell performance improvement.

2. Experimental

The anode NiO-ScSZ hollow fiber was produced by a phase-inversion method. NiO and ScSZ powders were mixed with ethanol by ball milling for 24 h and then dried. Polyethersulfone (PESf) was dissolved into

* Corresponding authors. Tel.: +1 803 777 4875.
E-mail addresses: esyangc@scut.edu.cn (C. Yang), chenfa@cec.sc.edu (F. Chen).

1388-2481/$ – see front matter © 2013 Elsevier B.V. All rights reserved.
http://dx.doi.org/10.1016/j.elecom.2013.06.015

N-methyl-2-pyrrolidone (NMP) to form a spinning solution. NiO-ScSZ powders were added into PESf-NMP spinning solution (weight ratio of NiO-ScSZ to PESf-NMP equals 1:1) and ball-milled to obtain viscous slurry. A custom designed spinneret with an orifice dimension/inner diameter of 3.0/2.0 mm was used to obtain a NiO-ScSZ fiber tube precursor. The NiO-ScSZ fiber tube precursor was immersed immediately into water bath to produce the porous NiO-ScSZ fiber tube precursor. The asymmetric porous fiber tube precursor was fired at 1200 °C for 2 h to remove organic binder. A thin ScSZ membrane electrolyte was then coated onto the pre-fired NiO-ScSZ fiber by a dip coating method. ScSZ-graphite ink (weight ration of ScSZ to graphite is 1:2) was then printed onto the ScSZ membrane electrolyte surface. After sintering at 1500 °C for 4 h, a porous layer of ScSZ matrix and a dense ScSZ membrane electrolyte architecture were obtained on porous NiO-ScSZ fiber. Subsequently, aqueous solution of $La(NO_3)_3 \cdot 6H_2O$ (1 mol L^{-1}), $Sr(NO_3)_2$ (1 mol L^{-1}), and $Mn(NO_3)_2 \cdot 4H_2O$ (1 mol L^{-1}) (with a mole ratio of La:Sr:Mn equals 0.7125:0.2375:1) to yield a composition of $(La_{0.75}Sr_{0.25})_{0.95}MnO_3$ was impregnated into porous ScSZ matrix, followed by decomposition of the nitrate at 800 °C for 0.5 h. After impregnation-heating cycles, ~30 wt.% LSM loading was achieved in the LSM-ScSZ electrode [15]. The LSM-ScSZ cathode was then impregnated by a 3 mol L^{-1} $Sm_{0.2}Ce_{0.8}(NO_3)_x$ solution, followed by firing at 800 °C for 0.5 h. After 4 cycles of impregnation, ~10 wt.% SDC loading was achieved in LSM-ScSZ-SDC layers. The prepared anode-supported MT-SOFC was 21 mm long with a cathode layer length of 9 mm and outside/inside diameter of ~1.5 mm/1.0 mm.

The MT-SOFC was connected and sealed to two alumina tubes at both ends, and placed on an alumina support in the furnace. The current density–voltage curves as well as the impedance spectra were measured with a four probe method using a multi-channel VersaSTAT (Princeton Applied Research) from 550 °C to 650 °C. After the fuel cell test, the microstructure of the MT-SOFC was characterized using a scanning electron microscope (SEM, FEI Quanta 200).

3. Results and discussion

3.1. Micro-structure of the MT-SOFCs

Fig. 1(a, b, c) shows the cross-sectional SEM images of the intermediate temperature Ni-ScSZ/ScSZ/LSM-SDC-ScSZ MT-SOFC. The thickness of the Ni-ScSZ anode is ~250 μm, dense ScSZ electrolyte film is ~20 μm and porous LSM-SDC-ScSZ is ~50 μm. The anode layer can be divided into two asymmetric layers, a layer with small finger-like pores close to the electrolyte serving as the anode function layer where electrochemical reaction takes place, while a layer with large finger-like pores serving as fuel delivery layer. The asymmetric porous hydrogen electrode microstructure in this work is very different from the previous report of intermediate temperature MT-SOFCs produced from the phase-inversion method [10]. In that report, the large finger-like pores are in the middle of the fuel electrode while the small finger-like pores are near the surface of the fuel electrode adjacent to the fuel flow region. Such microstructure is not effective for fuel delivery from the fuel flow region to the electrolyte/electrode reaction region and will consequently limit the cell performance. Since the fuel diffusion rate is proportional to the square of the porous anode geometrical tortuosity [16], it is expected that this unique microstructure will benefit the

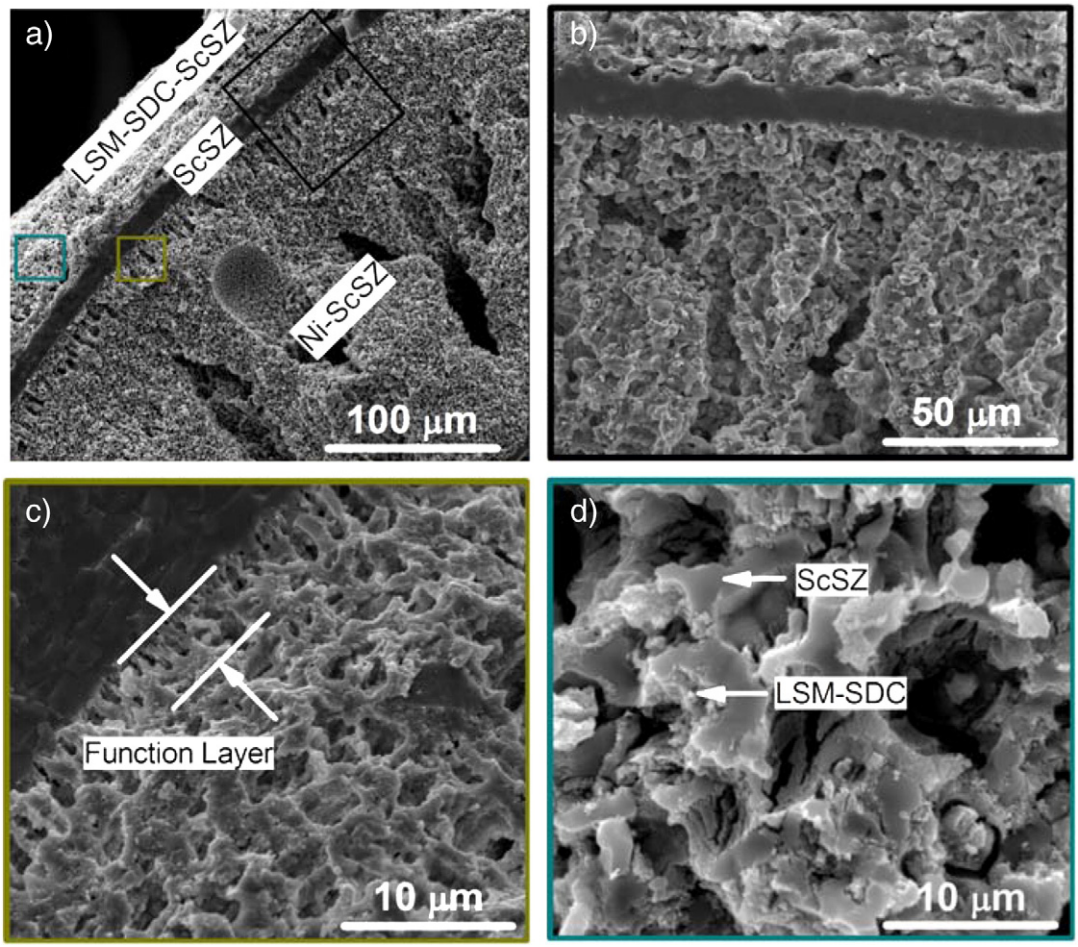

Fig. 1. a, b) Cross-sectional fracture surface micrograph of the anode-supported MT-SOFC, c) microstructure of the anode functional layer and anode fuel delivery layer, d) micro-structure of LSM-SDC infiltrated ScSZ cathode after fuel cell test.

fuel diffusion. Furthermore, it should be noticed that the small finger-like pores adjacent to the electrolyte layer allow the ScSZ slurry to penetrate into the Ni-ScSZ function layer during the dip-coating process for ScSZ electrolyte thin film preparation. Upon printing the ScSZ-graphite ink on the ScSZ electrolyte and co-sintering at high temperature, the dense ScSZ electrolyte and porous ScSZ backbone in the anode and cathode formed together (Fig. 1b). This microstructure is expected not only to provide optimized interface to facilitate oxygen ion conducting path, but also to alleviate the TEC mismatch among the cell components and improve the cell resistance to thermal cycling. Fig. 1(d) reveals the SEM image of LSM-SDC-ScSZ oxygen electrode. It can be seen that nano to sub-micro-sized LSM-SDC particles are homogenously coated on the ScSZ backbone from the infiltration process to form well-connected network.

3.2. Electrochemical performance of the MT-SOFCs

The polarization process of the fabricated Ni-ScSZ/ScSZ/LSM-SDC-ScSZ MT-SOFC has been investigated using electrochemical impedance spectra (EIS), as indicated in Fig. 2. H_2 flow rate was set at 30 standard cubic centimeters per minute (sccm). In the impedance spectra, the intercept on the real impedance axis at high frequency is related to the cell ohmic resistance (R_o), the intercept on the real impedance axis at low frequency is related to the total resistance (R_t), and the intercept on the real impedance axis between the high and low frequency is related to the cell polarization resistance (R_p). As the operating temperature increased from 550 to 650 °C, the R_t decreased from 1.2 to 0.59 Ω cm^2 while the R_o decreased from 0.6 to 0.33 Ω cm^2. The cell resistance obtained in this work is much lower than those reported for intermediate temperature MT-SOFCs with Ni-ScSZ/ScSZ/LSM-ScSZ configuration, where R_t is 3.49 Ω cm^2 with R_o of 1.14 Ω cm^2 at 700 °C [9] and R_t is 2.2 Ω cm^2 with R_o of 0.45 Ω cm^2 at 750 °C [17], and similar to the MT-SOFCs with the cell configuration of Ni-YSZ/Ni-ScSZ/ScSZ/LSM-ScSZ/LSM, where R_t is 0.8 Ω cm^2 with R_o of 0.177 Ω cm^2 at 650 °C [10]. However, the cell polarization resistance, R_p is about 0.26 Ω cm^2 at 650 °C in this study, which is much lower than that of the reported intermediate temperature MT-SOFCs with similar cell configurations fabricated by the phase-inversion method, where R_p is 0.623 Ω cm^2 at 650 °C [10]. Furthermore, the deposition of nano to sub-micro-sized LSM-SDC particles on the porous ScSZ surface would effectively increase the number of the cathode TPB sites for oxygen reduction compared with that obtained from a physically mixed process reported by Liu et al. [9] and Sun et al. [10]. Consequently, the cell polarization resistance is minimized, and the cell performance is substantially enhanced.

The voltage and power density curves as a function of current density at different temperatures for the MT-SOFC are shown in the inset in Fig. 2. Maximum power densities of 0.29, 0.40 and 0.52 W cm^{-2} have been obtained at 550, 600 and 650 °C, respectively. These maximum power densities are much higher than those of the anode-supported MT-SOFCs with ScSZ electrolyte, i.e., 0.38 W cm^{-2} at 650 °C reported by Sun et al. [10], 0.17 W cm^{-2} at 700 °C reported by Liu et al. [9], and that of the cathode-supported MT-SOFC, 0.15 W cm^{-2} at 650 °C reported by Yamaguchi et al. [8]. The fuel utilization can be calculated from the fuel flow rates and the current applied to the fuel cell. At the maximum cell power density, the fuel utilization of the MT-SOFCs is calculated to be 6.3%, 8.5% and 11.0% at 550, 600 and 650 °C, respectively.

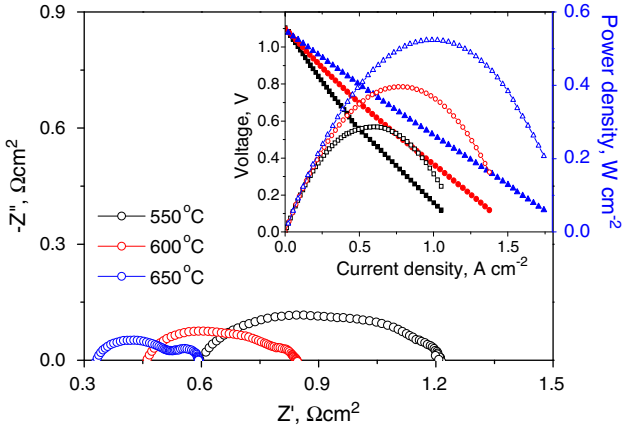

Fig. 2. Impedance spectra of Ni-ScSZ/ScSZ/LSM-SDC-ScSZ MT-SOFC measured under open circuit voltage (OCV) at 550, 600 and 650 °C. Inset shows the current density–voltage and power density curves for MT-SOFC tested from 550 °C to 650 °C.

3.3. Thermal cycling of MT-SOFCs

Finally, thermal and current load cycles have been performed from 200 to 650 °C in order to study the MT-SOFC stability, as shown in Fig. 3. The MT-SOFC was heated up to 650 °C and cooled down to 200 °C at a speed of 20 °C/min and the OCV and the maximum cell power density were monitored as a function of thermal cycles. The experimental value for OCV is about 1.1 V at 650 °C, very close to that predicted by the Nernst equation with 97% H_2–3% H_2O as fuel and ambient air as the oxidant, indicating that the ScSZ electrolyte films are crack-free. The maximum power densities of the MT-SOFC were around 0.5 W cm^{-2} at 650 °C, and the thermal cycles appear to have no adverse effect on the long-term performance of the MT-SOFCs, indicating that the unique microstructures of the MT-SOFCs studied in this work have excellent resistance to thermal cycling.

4. Conclusions

Ni-ScSZ/ScSZ/LSM-SDC-ScSZ intermediate temperature MT-SOFCs have been successfully fabricated and electrochemically studied in the temperature range from 550 to 650 °C. Cross-sectional SEM images of the fabricated MT-SOFC reveal that dense ScSZ electrolyte and porous ScSZ backbone in the anode and cathode formed together, and the MT-SOFCs have demonstrated robust resistance to thermal shock. The MT-SOFCs have achieved maximum power densities of 0.29, 0.40 and 0.52 W cm^{-2} at 550, 600 and 650 °C, respectively.

Acknowledgments

We gratefully acknowledge financial support of the South China University of Technology start-up fund, NASA EPSCoR (Award Number NNX10AN33A) and South Carolina Space Grant Consortium.

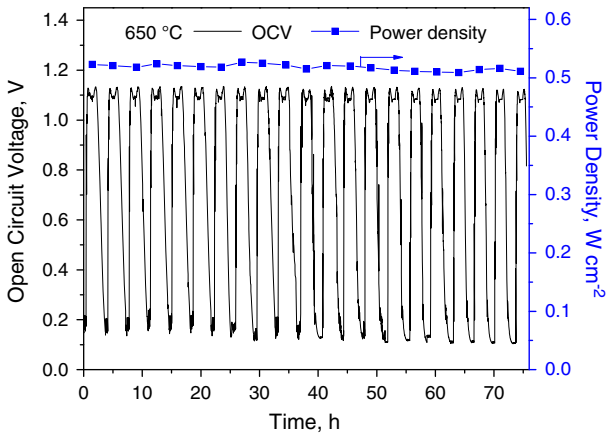

Fig. 3. Cell OCV and power output as a function of time in the thermal cycling experiments from 200 to 650 °C.

References

[1] S.M. Haile, Acta Materialia 51 (2003) 5981.
[2] E.P. Murray, T. Tsai, S.A. Barnett, Nature 400 (1999) 649.
[3] Y.H. Du, C. Finnerty, J. Jiang, Journal of the Electrochemical Society 159 (2008) B972.
[4] A.J. Jacobson, Chemistry of Materials 22 (2010) 660.
[5] X. Xue, J. Tang, N. Sammes, Y. Du, Journal of Power Sources 142 (2005) 211.
[6] K. Kendall, Solid Oxide Fuel Cell Structures, WIPO Patent Application, WO/1994/022178, 1994.
[7] S.C. Singhal, K. Kendall, High Temperature Solid Oxide Fuel Cells, Elsevier Science, Oxford, 2003.
[8] T. Suzuki, Z. Hasan, Y. Funahashi, T. Yamaguchi, Y. Fujishiro, M. Awano, Science 325 (2009) 852.
[9] R.Z. Liu, S.R. Wang, B. Huang, C.H. Zhao, J.L. Li, Z.R. Wang, Z.Y. Wen, T.L. Wen, Journal of Solid State Electrochemistry 13 (2009) 1905.
[10] W. Sun, N.Q. Zhang, Y.C. Mao, K.N. Sun, Electrochemistry Communications 20 (2012) 117.
[11] T. Suzuki, T. Yamaguchi, Y. Fujishiro, M. Awano, Journal of Power Sources 160 (2006) 73.
[12] R. Campana, A. Larrea, J.I. Pen, V.M. Orera, Journal of the European Ceramic Society 29 (2009) 85.
[13] D.H. Dong, M.F. Liu, K. Xie, J. Sheng, Y.H. Wang, X.B. Peng, X.Q. Liu, G.Y. Meng, Journal of Power Sources 175 (2008) 201.
[14] C.L. Yang, W. Li, S.Q. Zhang, L. Bi, R.R. Peng, C.S. Chen, W. Liu, Journal of Power Sources 187 (2009) 90.
[15] F. Zhao, Z.Y. Wang, M.F. Liu, L. Zhang, C.R. Xia, F.L. Chen, Journal of Power Sources 185 (2008) 13.
[16] R. O'Hayre, S.W. Cha, W. Colella, F.B. Prinz, Fuel Cell Fundamentals, 2nd ed. Wiley, 2008.
[17] H.X. Gu, R. Ran, W. Zhou, Z.P. Shao, Journal of Power Sources 172 (2007) 704.